Low Complexity FPGA Implementation of 2×2 MIMO-OTSM Transceiver for 6G Communications

Sapta Girish Neelam, *Senior Member, IEEE*
Centre of Excellence, Bharat Electronics Limited, India
E-mail : sgn10@iitbbs.ac.in

***Abstract*—A complete 2×2 single carrier Multiple Input Multiple Output (MIMO) modem was implemented on a Field Programmable Gate Array (FPGA) utilizing single-carrier modulation for operation under time varying channel conditions with limited mobility. To address real-world challenges, the receiver incorporates robust impairment mitigation techniques including compensation for In-phase/Quadrature (IQ) imbalance and Carrier Frequency Offset (CFO). Decision Feedback Equalization (DFE) driven by a Least Mean Squares (LMS) algorithm effectively counteracts the effects of multipath fading, inter-antenna interference, and spatial correlation, thereby enhancing overall signal quality. Robust timing recovery is achieved through a custom frame structure design coupled with a modified Gardner synchronization algorithm. While initial simulations were performed with a 2×2 system, the resulting architecture is readily scalable to support higher-order MIMO configurations. Simulation results demonstrate significant performance gains, particularly in environments with substantial inter-symbol interference (ISI) and strong spatial correlation, with single-user (SU) systems benefiting substantially from the integration of Maximal Ratio Combining (MRC).**

***Index Terms*—OTSM, LMS, OFDM, MIMO, MRC, OTFS.**

I. Introduction

As next-generation mobile networks evolve toward 6G and beyond, achieving reliable communication in highly dynamic environments is of paramount importance [1]. Orthogonal Time Frequency Space (OTFS) modulation has emerged as a promising alternative to traditional OFDM, offering improved robustness against aggressive channel variations inherent in mobile communications. OTFS accomplishes this by transforming the communication signal into the delay-Doppler domain, effectively realizing approximately flat fading characteristics and significantly mitigating inter-symbol interference [2]–[6]. This transformation inherently addresses the time-varying nature of wireless channels, offering a significant advantage over OFDM in high-mobility scenarios. Building upon this foundation, Orthogonal Time Sequency Multiplexing (OTSM) is particularly well-suited for linear time-varying (LTV) channels, leveraging the computational efficiency of the Walsh-Hadamard Transform (WHT) for waveform generation. Beyond its efficiency, OTSM exhibits inherent resilience to common receiver hardware imperfections such as IQ imbalance, making it attractive for practical implementation [7]–[9]. The simplicity of the WHT allows for efficient signal processing, reducing the computational burden on the receiver.

Recent research has focused on refining OTSM performance through the development of sophisticated channel estimation techniques, including iterative algorithms designed to overcome the challenges posed by noisy measurements and limited pilot sequences, and exploring optimized data detection strategies, initially within SISO systems [10]. Excitingly, MIMO-OTSM holds the potential to dramatically enhance spectral efficiency in future 6G deployments. Current investigations are actively extending MIMO-OTSM into challenging scenarios such as intelligent reflecting surface (IRS) assisted communication to combat path loss and enhance signal coverage, and employing distributed interference alignment precoding techniques for multi-user MIMO-OTSM downlink transmissions operating in time-varying channels [11], [12]. However, a rigorous theoretical and empirical performance analysis of MIMO-OTSM operating under quasi-static channel conditions remains a relatively unexplored area of research, hindering its widespread adoption.

In response to this critical need, this work which is implemented on FPGA introduces a low-complexity receiver architecture based on DFE for MIMO-OTSM in time varying environments, employing a computationally efficient LMS algorithm. This DFE-LMS combination provides adaptive interference cancellation, mitigating the effects of uncompensated inter-symbol interference and co-channel interference. Importantly, this approach is also readily applicable to SISO-OTSM systems [3], scales linearly with antenna array size for efficient implementation, and demonstrably improves SINR through iterative interference cancellation. The low computational complexity makes it suitable for resource-constrained mobile devices. Performance is thoroughly validated using a 2×2 MIMO configuration, providing strong evidence for the scalability of this architecture to higher-order MIMO systems. A detailed performance analysis, including timing synchronization and equalization will be presented below.

II. System Model of MIMO-OTSM

Fig. 1 illustrates the system model, which employs a Timing synchronization module and LMS-based DFE in a $n_T \times n_R$ MIMO configuration over a LTV channel.

A. MIMO-OTSM Transmitter and Receiver

In the MIMO-OTSM system (Fig. 1), signals are represented in the delay-sequency (DS) domain by $\mathbf{X}_{\mathrm{DS}}^{(t)}$ for the transmitted signal and $\mathbf{Y}_{\mathrm{DS}}^{(r)}$ for the received signal. These matrices consist of M delay bins and N sequency bins, mediating the signal's representation between time and frequency. The WHT serves as the core mathematical tool for efficient

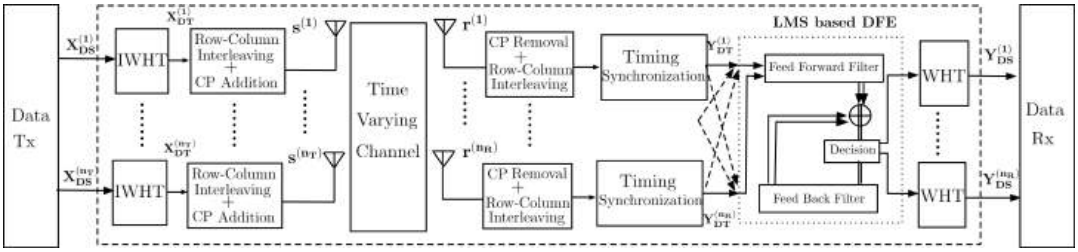

Fig. 1. System model of MIMO-OTSM with LMS based Decision Feedback Equalizer.

conversion between the DS and time domain representations. Higher-dimensional WHT matrices are recursively generated through tensor products: $\mathrm{W}_N = \mathrm{W}_2 \otimes \cdots \otimes \mathrm{W}_2$ (n times). Consequently, the time-domain signals at the transmitter and receiver are obtained via the inverse WHT operation applied to the DS domain signals:

$$\begin{aligned} \mathbf{s}^{(t)} &= \mathrm{vec}(\mathbf{X}_{\mathrm{DS}}^{(t)} \cdot \mathbf{W}_N^{\dagger}) = [\widetilde{\mathbf{x}}_0^{(t)}, \widetilde{\mathbf{x}}_1^{(t)}, \ldots, \widetilde{\mathbf{x}}_{M-1}^{(t)}]^T, \\ \mathbf{r}^{(r)} &= \mathrm{vec}(\mathbf{Y}_{\mathrm{DS}}^{(r)} \cdot \mathbf{W}_N^{\dagger}) = [\widetilde{\mathbf{y}}_0^{(r)}, \widetilde{\mathbf{y}}_1^{(r)}, \ldots, \widetilde{\mathbf{y}}_{M-1}^{(r)}]^T. \end{aligned} \tag{1}$$

Finally, to combat the effects of ISI and ensure dependable data reception, a cyclic prefix of length L_G carefully chosen to exceed the channel's maximum delay spread is prepended to each transmitted frame.

B. Linear Time Varying Channel

In a MIMO system operating in a multipath environment, the wireless channel between transmitter t and receiver r is characterized by a time-varying impulse response, denoted as $h^{(r,t)}(\tau, \nu)$. This response encapsulates the impact of numerous signal paths, each defined by its complex path gain, propagation delay (τ), and Doppler shift (ν). The channel's representation in the delay-Doppler (DD) domain is mathematically expressed as:

$$h^{(r,t)}(\tau, \nu) = \sum_{j=1}^{P^{(r,t)}} h_j^{(r,t)} \delta(\tau - \tau_j^{(r,t)}) \delta(\nu - \nu_j^{(r,t)}) \tag{2}$$

where $P^{(r,t)}$ signifies the total number of distinct multipath components contributing to the channel. The term $h_j^{(r,t)}$ represents the complex attenuation and phase shift introduced by the j-th path. To obtain the time-domain channel impulse response, which describes the channel's behavior as a function of time, we perform an inverse Fourier transform on the DD representation:

$$g^{(r,t)}(\tau, \overrightarrow{t}) = \int_{\nu} h^{(r,t)}(\tau, \nu) e^{j2\pi\nu(\overrightarrow{t} - \tau)} d\nu. \tag{3}$$

This transforms the channel description from the frequency domain (delay and Doppler) to the time domain. For practical implementation in digital communication systems, the continuous-time channel model is discretized. Applying a sampling interval of $1/(M\Delta f)$ and evaluating the integral at discrete time and delay instances, $\tau = l/(M\Delta f)$ and $\overrightarrow{t} = q/(M\Delta f)$, results in the discrete-time channel model:

$$g^{(r,t)}[\ell, q] = \sum_{j=1}^{P^{(r,t)}} h_j^{(r,t)} z^{(q-\ell)\kappa_j^{(r,t)}} \delta[\ell - \ell_j^{(r,t)}]. \tag{4}$$

Here, ℓ and q denote the discrete delay and time indices, respectively. $\ell_j^{(r,t)}$ represents the discrete delay index of the j-th path, and $z = \exp(j\frac{2\pi}{MN})$ is the phase rotation factor, accounting for the Doppler shift in the discrete-time domain. Finally, $\kappa_j^{(r,t)}$ denotes the discrete Doppler shift associated with the j-th path. This discretized model enables efficient signal processing algorithms for channel estimation, equalization, and precoding in MIMO communication systems.

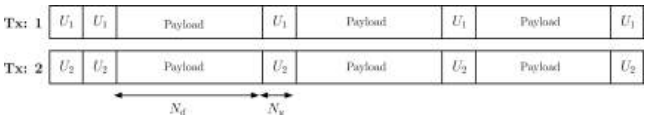

Fig. 2. Frame structure for 2×2 MIMO.

C. Spatial Correlation Modelling

In MIMO systems, spatial correlation among sub-channels (r, t) significantly influences system performance. This correlation stems from antenna characteristics, transceiver geometries, and the propagation environment. We quantify this correlation using transmitter and receiver correlation matrices, $\mathbf{R}_{\mathrm{t}}$ and $\mathbf{R}_{\mathrm{r}}$, respectively, employing a standard receive correlation matrix formulation. Specifically, the receiver correlation matrix is given by [13]:

$$\mathbf{R}_{\mathrm{r}} = \mathrm{Toep}\left(1, b, b^2, \ldots, b^{n_r - 1}\right) = \mathbf{L}_{\mathrm{r}} \mathbf{L}_{\mathrm{r}}^{\dagger} \tag{5}$$

where $\mathbf{L}_{\mathrm{r}}$ is a lower triangular matrix from the Cholesky decomposition of $\mathbf{R}_{\mathrm{r}}$. The correlation coefficient b is defined as $b = \rho_r^{\frac{1}{n_r - 1}}$, with $\rho_r \in (0, 1)$ representing the spatial correlation degree at the receiver. Note that $\mathbf{L}_{\mathrm{r}} \in \mathbb{R}^{n_r \times n_r}$ indicates real-valued components and dimensions $n_r \times n_r$. Analogously, substituting ρ_{r} with ρ_{t} yields the transmitter's correlation matrix, $\mathbf{R}_{\mathrm{t}}$. To model the complex baseband channel matrix $\mathbf{A}_j$ of size $n_R \times n_T$, we initially assume independent and identically distributed (i.i.d.) complex Gaussian entries: $\mathbf{A}_j[r, t] \sim \mathcal{CN}(0, \sigma_j^2(r, t))$, where $\sigma_j^2(r, t)$ is the average power of the j-th path in sub-channel (r, t). However, we refine this to account for real-world spatial correlation. The channel coefficients are therefore defined as:

$$\bar{\mathbf{A}}_j = \mathbf{L}_{\mathrm{r}} \cdot \mathbf{A}_j \cdot \mathbf{L}_{\mathrm{t}}^{\dagger} \tag{6}$$

where $\bar{\mathbf{A}}_j$ represents the spatially correlated channel matrix. This formulation introduces correlation by transforming the i.i.d. channel matrix $\mathbf{A}_j$ via the receiver and transmitter Cholesky factors, $\mathbf{L}_{\mathrm{r}}$ and $\mathbf{L}_{\mathrm{t}}^{\dagger}$, respectively, ensuring $\bar{\mathbf{A}}_j$ reflects the correlation from $\mathbf{R}_{\mathrm{t}}$ and $\mathbf{R}_{\mathrm{r}}$.

D. Input-Output Relations

In a discrete-time (DT) MIMO system, the received signal is modelled as a superposition of contributions from all transmitted signals, corrupted by additive noise. A crucial

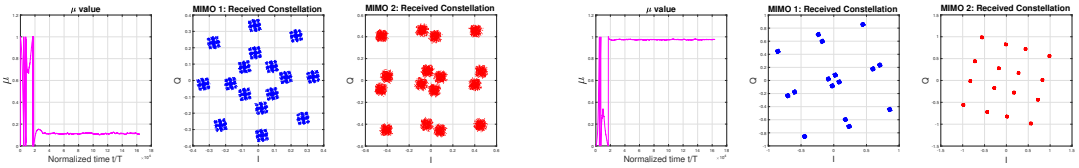

Fig. 3. Timing Synchronization results at time instants $t = \tau_1, t = \tau_2$ for spatially correlated 2×2 MIMO-OTSM with QPSK modulation.

factor affecting performance is the presence of Carrier Frequency Offset (CFO), which introduces a phase shift into the transmitted signal. Mathematically, this is expressed as:

$$\widetilde{\mathbf{r}}^{(r)}[q] = \sum_{t=1}^{n_{\mathrm{T}}} \sum_{\ell \in \mathcal{L}^{(r,t)}} \widetilde{g}^{(r,t)}[\ell, q]\mathbf{s}^{(t)}[q-\ell] + \mathbf{z}^{(r)}[q], \quad (7)$$

where $\widetilde{g}^{(r,t)}[\ell, q]$ encapsulates the channel response, including the phase shift induced by CFO, and $\mathcal{L}^{(r,t)}$ is the set of delays representing the propagation time between transmitter t and receiver r.

E. Frame Structure for 2×2 MIMO-OTSM

The frame structure for 2×2 MIMO is illustrated in Fig. 2. Each transmit signal $\mathbf{x}_i \in \mathbb{C}^{2N_u+BN}$ consists of:

$$\mathbf{x}_i = \begin{bmatrix}\mathbf{x}_{p,i}^T & \mathbf{x}_d^T & \mathbf{x}_{u,i}^T & \cdots & \mathbf{x}_d^T & \mathbf{x}_{u,i}^T\end{bmatrix}^T \quad (8)$$

where $\mathbf{x}_d \in \mathbb{C}^{N_d}$ is the payload sequence, $\mathbf{x}_{p,i}$ represents the preamble sequence, and B denotes the number of transmission blocks, each of size $N = N_d + N_u$.

III. MIMO Timing Synchronization Algorithm

Precise symbol, carrier, and phase synchronization are essential for accurate digital demodulation. Feedback-based synchronization, employing a phase-locked loop, generally yields superior performance but necessitates a settling time. Crucially, accurate equalization relies on stable symbol synchronization, achieved through timing error correction to sample at the optimal time instance (center of the eye diagram). Performance at low SNR is further improved by prefiltering. Timing synchronization is done independently for every received channel and the sequence of steps are listed below.

A. Linear Interpolation

Digital interpolation is performed using a linear interpolator, chosen for its computational efficiency. Linear interpolation at each antenna j generates interpolants via:

$$\mathbf{y}^j(kT_i) = \mathbf{y}^j[(m_k+\mu_k^j)T] = \sum_{i=I_1}^{I_2} \mathbf{r}^j[(m_k-i)T]h_I[(i+\mu_k^j)T]$$

where T is the sampling interval, μ_k is the fractional interval, m_k is the basepoint index, and $h_I(t)$ is the finite-duration impulse response. I_1 and I_2 define the summation limits.

B. Timing Error Detection (T.E.D) and Loop Filter

Timing error is defined as sampling the eye diagram away from its center, maximizing average eye opening. The Gardner algorithm is employed to calculate the timing error, $\mathbf{E}^j[k]$:

$$\mathbf{E}^j[k] = \mathbf{y}^j[k-0.5](\mathbf{y}^j[k] - \mathbf{y}^j[k-1]) \quad (9)$$

The timing error, $\mathbf{E}^j[k]$, is processed by a proportional-plus-integral (Type II) loop filter to control the NCO. Key parameters are tuned using classical PLL theory, with a noise bandwidth B_nT set to 5% of the symbol rate and a damping factor of 0.707. The loop filter update equation is:

$$\mathbf{L}^j[k] = \mathbf{L}^j[k-1] + (K_1+K_2)\mathbf{E}^j[k] - K_1\mathbf{E}^j[k-1] \quad (10)$$

where K_1, K_2 are constants derived based on loop parameters.

C. Interpolation Control (NCO)

Interpolation timing is controlled by a numerically controlled oscillator (NCO) operating at the symbol rate. The NCO's register content, $\eta^j[k]$, and control word, $\mathbf{W}^j[k]$, determine the fractional interval μ_k. The NCO updates as

$$\eta^j[k] = \eta^j[k-1] - \mathbf{W}^j[k-1] \bmod -1 \quad (11)$$

A decrementing NCO simplifies the computation of μ_k^j. The loop filter adjusts $\mathbf{W}^j[k]$ to accurately time the interpolator output. Given an oversampling factor N, we have $\mathbf{W}^j[k] = \frac{1}{N} + \mathbf{L}^j[k]$. Under stable loop conditions, $\mathbf{W}^j[k]$ is nearly constant. To avoid division in FPGA implementation, μ_k^j is approximated as $\mu_k^j = \eta^j[k]\widetilde{M}$, where $\widetilde{M}$ is a scaling factor. An underflow signal is asserted when $\eta^j[k]$ reaches 0, generating timing strobes for interpolating the filtered waveform.

IV. MIMO Adaptive DFE Algorithm

The MIMO Adaptive DFE algorithm, designed for QPSK constellation demodulation, operates on time synchronized received signals $\mathbf{y}_1(n)$ and $\mathbf{y}_2(n)$, leveraging a pre-defined transmit constellation $\mathcal{TX}_{const}$ and a tunable learning step size μ. The algorithm dynamically estimates the transmitted QPSK symbols through an iterative process of signal combination, adaptive filtering, and feedback. Initially, the input signals are linearly combined using weights $\mathbf{W}_{11}, \mathbf{W}_{22}, \mathbf{W}_{21}, \mathbf{W}_{12}$ to generate intermediate outputs:

$$\mathbf{Y}_1 = \mathbf{W}_{11}\mathbf{y}_1 + \mathbf{W}_{21}\mathbf{y}_2$$
$$\mathbf{Y}_2 = \mathbf{W}_{12}\mathbf{y}_1 + \mathbf{W}_{22}\mathbf{y}_2$$

Concurrently, a decision feedback mechanism employing adaptive weights $\mathbf{W}_{\mathrm{FB}_{11}}, \mathbf{W}_{\mathrm{FB}_{12}}, \mathbf{W}_{\mathrm{FB}_{21}}, \mathbf{W}_{\mathrm{FB}_{22}}$ extracts information from past output decisions, effectively mitigating inter-symbol interference. These intermediate outputs, $\mathbf{Y}_1$ and $\mathbf{Y}_2$, are subsequently quantized to the nearest point within the known $\mathcal{TX}_{const}$, yielding estimated QPSK symbols $\mathbf{d}_1(n)$ and $\mathbf{d}_2(n)$. The adaptive weights are then refined using the Least Mean Squares (LMS) algorithm. Specifically:

$$\mathbf{W}_{11}(n+1) = \mathbf{W}_{11}(n) + \mu\,\mathbf{er_1}(n)\,\mathbf{y}_1(n),$$
$$\mathbf{W}_{21}(n+1) = \mathbf{W}_{21}(n) + \mu\,\mathbf{er_1}(n)\,\mathbf{y}_2(n),$$
$$\mathbf{W}_{12}(n+1) = \mathbf{W}_{12}(n) + \mu\,\mathbf{er_2}(n)\,\mathbf{y}_1(n),$$
$$\mathbf{W}_{22}(n+1) = \mathbf{W}_{22}(n) + \mu\,\mathbf{er_2}(n)\,\mathbf{y}_2(n),$$

Algorithm 1 2x2 MIMO Adaptive DFE Receiver

Input: Received symbols $\mathbf{y}_1(n), \mathbf{y}_2(n)$.
Output: Estimated symbols $\hat{\mathbf{s}}_1, \hat{\mathbf{s}}_2$.

Initialization: Initialize adaptive and feedback filter weights $\mathbf{W}_{ij}$, $\mathbf{W}_{\text{FB}_{ij}}$, and transmit constellation TX_{const} for $i, j \in \{1, 2\}$.
while $n < N_{Tr}$ **do**
  Mixing: Calculate $\mathbf{Y}_i$ by mixing $\mathbf{y}_1, \mathbf{y}_2$ with channel coefficients.
  Filtering: Compute $\mathbf{Y}_i$ using adaptive and feedback filtering of $\mathbf{y}_i$ with $\mathbf{W}_{ij}$ and $\mathbf{W}_{\text{FB}_{ij}}$, respectively.
  QPSK Decision: $\hat{\mathbf{s}}_i \leftarrow \text{argmin}_{\mathbf{s} \in \text{TX}_{\text{const}}} \|\mathbf{Y}_i - \mathbf{s}_i\|$ for $i = 1, 2$.
  Error Calculation:
  if Training Mode **then**
    $\mathbf{er}_i(n) \leftarrow \mathbf{Y}_i(n) - \mathbf{d}_i(n)$
  else
    $\mathbf{er}_i(n) \leftarrow \mathbf{Y}_i(n) - \text{TX}_{\text{const}}(\hat{\mathbf{s}}_i(n))$
  end if
  Weight Update: Update $\mathbf{W}_{ij}$ and $\mathbf{W}_{\text{FB}_{ij}}$ using $\mathbf{er}_1(n)$ and $\mathbf{er}_2(n)$ (e.g., LMS).
  VCO Update: Update VCO based on data.
end while

TABLE I
COMPUTATIONAL COMPLEXITY COMPARISON OF SISO/MIMO-DFE

System	Multipliers	Adders
SISO	$N_{FF} + N_{FB} + 1$	$N_{FF} + N_{FB}$
MIMO (2×2)	$4(N_{FF} + N_{FB} + 1)$	$2(2N_{FF} + 2N_{FB} + 1)$

and similarly for the feedback weights $\mathbf{W}_{\text{FB}_{11}}$, $\mathbf{W}_{\text{FB}_{12}}$, $\mathbf{W}_{\text{FB}_{21}}$, $\mathbf{W}_{\text{FB}_{22}}$ respectively. The algorithm's learning process is bifurcated into two phases: a training phase, conducted over $N_{\text{Tr}} <$ Trng samples utilizing the known transmitted symbols to calculate errors, and a decision phase, where indexing is used to determine the error signals $\mathbf{er}_1(n)$ and $\mathbf{er}_2(n)$. The LMS algorithm then utilizes these calculated errors to iteratively update the adaptive weights. Finally, the recovered signal is generated by multiplying with an updated Voltage-Controlled Oscillator (VCO) using the quantized outputs, resulting in $\mathbf{Y}_1$ and $\mathbf{Y}_2$, a detailed breakdown of this process is provided in Algorithm 1. The system employs an iterative joint adaptation algorithm for equalization and carrier recovery. The computational complexity comparison of SISO DFE and MIMO-DFE is shown in Table 1, where N_{FF}, N_{FB} indicates number of feed-forward and feedback taps. The complexity scales with the MIMO order.

V. RESULTS AND ANALYSIS

This section details the simulation and implementation on Matlab/FPGA, its methodology and parameters used to evaluate the performance of a MIMO-OTSM system utilizing LMS based DFE detection. System parameters were established as follows: $M = 128$ delay bins and $N = 128$ sequency bins, operating at a carrier frequency of 4 GHz with a subcarrier spacing of 15 KHz. Channel characteristics were modelled using the Vehicular channel profile, incorporating twelve distinct multi-path components to represent a realistic vehicular communication environment. Mobility was simulated with a maximum vehicular speed of 72 km/hr, inducing Doppler shifts treated as independent and uniformly distributed across each propagation path. Feed forward and feedback tap lengths were both set to 16. A comprehensive summary of all simulation parameters is provided in Table II. The algorithms were first simulated in Matlab and subsequently implemented on an FPGA for real-time operation.

TABLE II
MATLAB/FPGA BASED SIMULATION PARAMETERS FOR MIMO-OTSM

Sim./Emu. Parameter	Sim./Emu. Value
$f_c, P, M, N, \Delta f$	4 GHz, 12, 128, 128, 15 kHz
Timing Synchronization	Modified Gardner
Data Detectors	LMS DFE
PDP (dB) for MIMO 1, 2	[0, -9, -18, -27, -36, -40]
Delay taps for MIMO 1, 2	[0, $\frac{T_s}{2}$, 1.0 T_s, 3 $\frac{T_s}{2}$, 2.0 T_s, 5$\frac{T_s}{2}$]
ρ_{rx}	[0, 0.2, 0.4, 0.6, 0.8, 0.9]
Feedback, FeedForward Taps	16, 16
Mobility, Fading Type	72 Km/hr, Rayleigh

A. Matlab based Results

To further illustrate the capabilities of the MIMO-OTSM framework, Fig. 4 presents the performance of Quadrature Phase-Shift Keying (QPSK) symbol equalization within a 2×2 MIMO system. This figure compares the performance with and without equalization, highlighting the associated feed-forward weights employed in the equalized scenario. The plot illustrates the convergence of the weights in both the channels for MIMO 1 and MIMO 2. A key observation from the results is the robustness of the equalization performance to variations in the receive spatial correlation; the performance is largely unaffected by changes in this parameter. Beyond the final equalization accuracy, Fig. 4 also characterizes the transient and steady-state behavior of the system. The plot reveals a relatively rapid convergence, with effective training achieved using a limited number of symbols, demonstrating the practical feasibility of the proposed approach. The power delay profile (PDP), expressed in dB, and the corresponding path delays (in symbol times) are listed in Table II.

B. FPGA based Results

The performance of a 2×2 MIMO system implemented on FPGAs is demonstrated in Fig. 5. Following root-raised cosine filtering, symbol synchronization is independently performed on each data stream. These time synchronized symbols are then passed to the MIMO equalizer for equalization. Data was transmitted and received using FPGAs, with a channel emulator simulating realistic channel conditions, as detailed by the parameters in Table II. Fig. 5(a) illustrates the channel equalization process, showing the convergence of channel estimates and the stabilization of the adaptive weights (both feed-forward and feed-back). Constellation diagrams before and after equalization are presented in Fig. 5(b) and (c) for MIMO channel 1, and in Fig. 5(d) and (e) for MIMO channel 2. Importantly, Fig. 5(b) and (d) display the constellations

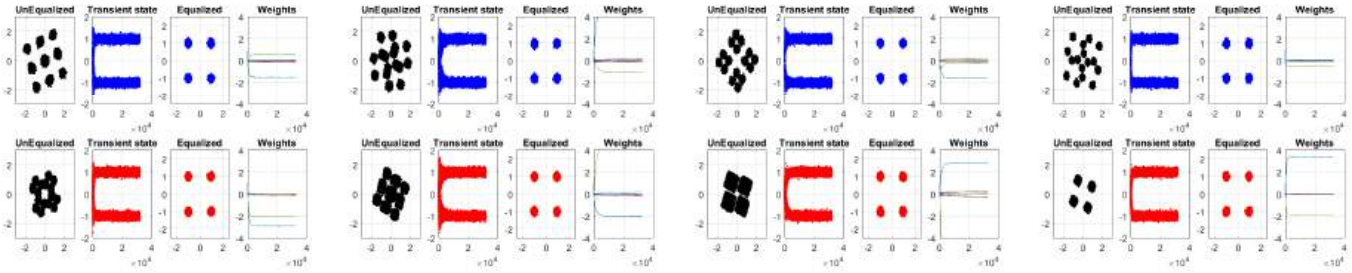

(a) $\rho_r = 0.0$ (b) $\rho_r = 0.2$ (c) $\rho_r = 0.4$ (d) $\rho_r = 0.6$

Fig. 4. **Matlab** based Simulation Performance was evaluated for spatially correlated 2×2 MIMO-OTSM with QPSK modulation, utilizing $N = 128$ and $M = 128$ with varying antenna correlation ρ_r at SNR of 20 dB.

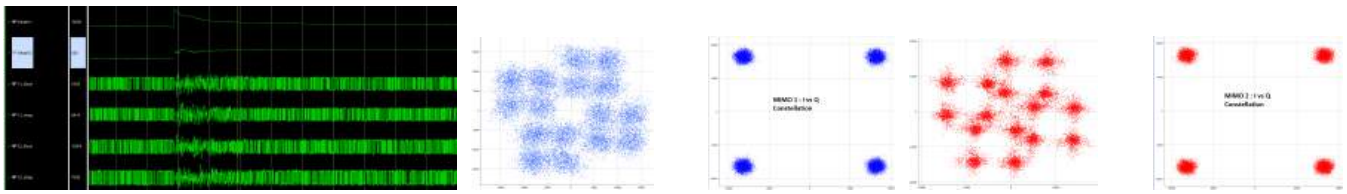

(a) 2×2 MIMO results from FPGA under time varying Channel at **time** t_0 (b) MIMO 1: **Before** Equalization (c) MIMO 1: **After** Equalization (d) MIMO 2: **Before** Equalization (e) MIMO 2: **After** Equalization

Fig. 5. **FPGA** based real time performance was evaluated for spatially correlated 2×2 MIMO-OTSM with QPSK modulation, at SNR of 20 dB.

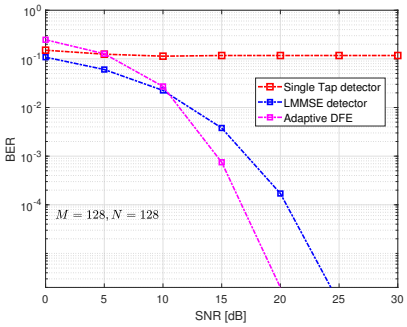

Fig. 6. Comparison of BER vs SNR for 2×2 MIMO OTSM with various detectors.

after timing synchronization, which were then fed into the adaptive Decision Feedback Equalization (DFE) algorithm. The results indicate successful elimination of inter-antenna interference, alongside compensation for multipath fading and mild Doppler shifts. BER vs SNR for 2×2 MIMO is plotted in Fig. 6, which clearly indicates that our detector performs better than Single tap and LMMSE detectors. Another feed-forward equalizer, employing only its weights and considering both the signal and its conjugate, effectively mitigates IQ-imbalance.

VI. Conclusion

In conclusion, this work has demonstrated a practical and effective detection strategy for MIMO-OTSM systems, capable of mitigating the effects of realistic channel impairments. The integration of a low-complexity DFE with LMS adaptation provides a robust solution, particularly benefiting performance in spatially correlated environments. Simulation and FPGA-based validation confirm significant gains over conventional schemes, paving the way for the deployment of high-performance, reliable MIMO-OTSM communication in practical applications. Future work will focus on extending this approach to multi-user scenarios and exploring advanced adaptation algorithms for further performance enhancement.

References

[1] F. Hlawatsch and G. Matz, Eds., *Wireless Communications Over Rapidly Time-Varying Channels*. New York, NY, USA: Academic, 2011.

[2] R. Hadani *et al*., "Orthogonal time frequency space modulation," in *Proc. IEEE Wireless Commun. Netw. Conf. (WCNC),* Mar. 2017, pp. 1–6.

[3] T. Thaj and E. Viterbo, "Low complexity iterative rake decision feedback equalizer for zero-padded OTFS systems", *IEEE Trans. Veh. Technol.,* vol. 69, no. 12, pp. 15606-15622, Dec. 2020.

[4] T. Thaj and E. Viterbo, "Low-Complexity Linear Diversity-Combining Detector for MIMO-OTFS," in *IEEE Wireless Commun. Lett.*, vol. 11, no. 2, pp. 288-292, Feb. 2022, doi: 10.1109/LWC.2021.3125986.

[5] S. G. Neelam and P. R. Sahu, "Analysis, Estimation and Compensation of Hardware Impairments for CP-OTFS Systems," in *IEEE Wireless Commun. Lett.*, vol. 11, no. 5, pp. 952-956, May 2022.

[6] S. G. Neelam and P. R. Sahu, "Digital Compensation of IQ Imbalance, DC offset for Zero-Padded OTFS Systems," *IEEE Commun Lett.*, vol. 26, no. 10, pp. 2450-2454, Oct. 2022.

[7] S. G. Neelam and P. R. Sahu, "Estimation and Compensation of IQ Imbalance for OTSM Systems," *IEEE Wireless Commun. Let.*, 2022, vol. 11, no. 9, pp. 1885-1889, Sept. 2022.

[8] S. G. Neelam and P. R. Sahu, "Joint compensation of TX/RX IQ imbalance and channel parameters for OTSM systems," *IEEE Commun. Lett*., vol. 27, no. 3, pp. 976–980, Mar. 2023, doi: 10.1109/LCOMM.2023.3234538.

[9] S. G. Neelam and P. R. Sahu, "Joint Estimation and Compensation of CFO, IQ Imbalance and Channel Parameters for Zero Padded OTSM Systems,"*IEEE Commun. Lett*., vol. 12, no. 11, pp. 1871-1875, Nov. 2023, doi: 10.1109/LWC.2023.3297133.

[10] S. G. Neelam and P. R. Sahu, "Iterative channel estimation and data detection of OTSM with superimposed pilot scheme and PAPR analysis," *IEEE Commun. Lett*., vol. 27, no. 8, pp. 2147–2151, Aug. 2023, doi:10.1109/LCOMM.2023.3281575.

[11] S. G. Neelam, "Spatially Correlated SU MIMO-OTSM: Performance Analysis," *IEEE Commun. Lett*., vol. 28, no. 8, pp. 1944-1948, Aug. 2024, doi: 10.1109/LCOMM.2024.3420115.

[12] S. Nalluru and S. G. Neelam, "Low Complexity Detection of IRS-Aided MIMO-OTSM Under Perfect Phase Optimization," *IEEE Commun. Lett*., vol. 29, no. 2, pp. 393-397, Feb. 2025, doi: 10.1109/LCOMM.2024.3520700.

[13] A. S. Bora, K. T. Phan, and Y. Hong, "Mitigating spatial correlation in MIMO-OTFS," *IEEE Trans. Veh. Technol*., vol. 73, no. 3, pp. 3608–3622, Mar. 2024, doi: 10.1109/TVT.2023.3324925.